applied sciences

MDPI

Article

Comparison of Temperature Characteristics of Outer Rotor Low-Speed PM Motors Considering Magnetic Load and Current Density

Guanghui Du *, Qizheng Zhang, Qixun Zhou, Chengshuai Hu and Tao Pu

School of Electrical and Control Engineering, Xi'an University of Science and Technology, Xi'an 710054, China
* Correspondence: duguanghui1104@163.com

Abstract: In the electromagnetic design process of the outer rotor of a low-speed permanent magnet motor (LSPMM), due to the different heat dissipation conditions of the stator core and the stator winding, the selection of different magnetic loads and stator current densities will produce different temperature distributions even under the same efficiency. In the existing literature, the effects of magnetic load and current density on temperature distribution are rarely studied, which makes it difficult for designers to select optimal electromagnetic parameters to achieve better temperature performance. Therefore, in this paper, the comparison of temperature characteristics considering magnetic load and current density is conducted based on an outer rotor LSPMM. Firstly, the structure and parameters of an initial scheme of a 200 kW 56 rpm motor is determined, and the electromagnetic and temperature characteristics of the initial scheme are obtained through two-dimensional finite element analysis (2D-FEA) using Ansys Maxwell and Motor-CAD software. Secondly, by comparing the temperature and loss characteristics under different magnetic loads and different current densities, the effect of magnetic load on temperature and the effect of current density on temperature are obtained. Furthermore, four different schemes are proposed, and the loss and temperature characteristics of the four schemes under rated load are also compared to obtain the comprehensive effects of magnetic load and current density on temperature. Next, a final scheme is determined based on the above analysis, and the temperature characteristics of the final scheme and the initial scheme are compared to verify the validity of the conclusions. Finally, a prototype is built and tested to verify the feasibility of the conclusions. For LSPMM design, the results and several measurements provided in this paper can help researchers to choose a better optimization scheme to achieve good temperature performance.

Keywords: outer rotor; low-speed permanent magnet motor; magnetic load; current density; temperature comparison

Citation: Du, G.; Zhang, Q.; Zhou, Q.; Hu, C.; Pu, T. Comparison of Temperature Characteristics of Outer Rotor Low-Speed PM Motors Considering Magnetic Load and Current Density. *Appl. Sci.* **2022**, *12*, 8339. https://doi.org/10.3390/app12168339

Academic Editors: Gang Lei, Jianguo Zhu, Youguang Guo and Yujiao Zhang

Received: 27 July 2022
Accepted: 18 August 2022
Published: 20 August 2022

1. Introduction

LSPMMs are widely used in industrial production, oil field exploration, wind power generation, port lifting, and ship propulsion [1,2]. The traditional drive system of an induction motor plus a mechanical deceleration mechanism has disadvantages, such as complex structure, leakage of lubricating oil, poor operation reliability, high maintenance cost, and low overall efficiency of the system; thus, this system does not meet the requirements of economic development, energy saving, and environmental protection [3,4]. The use of direct drive motors to replace traditional drive systems has become the consensus of scholars at home and abroad [5]. In addition, the power factor and efficiency of permanent magnet motors are higher, and permanent magnet motors can maintain good performance over a wide range of load changes [6]. Therefore, LSPMMs are wildly used. However, an LSPMM needs to output a large torque, and it will generate a large electromagnetic torque, resulting in a large magnetic load and copper loss [7]. On the other hand, the lower speed

results in less effective self-fan cooling, causing the high-temperature rise of the motor [8]. The higher motor temperature can result in the permanent magnet (PM) undergoing demagnetization and, ultimately, worse motor performance [9]. Hence, for LSPMMs, the suitable temperature is significant for guaranteeing good motor operating conditions.

For LSPMMs, most of the literature focuses on motor design and performance optimization. An LSPMM with fractional concentrated winding used in a coal mine conveyor belt system was designed, of which the temperature distribution of different conductor turns and permanent magnet materials are presented in [10]. A new stator cooling structure design was studied to achieve a lower temperature rise, and the results show that the larger magnetic load and lower current density can improve torque density [11]. The U-shaped hybrid pole is proposed to improve motor torque density in [12]. The effects of stator tooth shape on output torque and bearing stress have also been studied, based on a bearingless outer rotor of a permanent magnet synchronous motor [13]. Furthermore, the effects of pole pair number and winding type on motor performance were investigated in [14]; a suitable embrace was found in order to obtain minimum cogging torque in [15]; and the influence of ratio of external diameter to stack length on torque and efficiency was analyzed in [16]. In the electromagnetic design of LSPMMs, the selection of magnetic load and current density has a great influence on electromagnetic performance. Magnetic load mainly affects the rotor core loss, eddy current loss of the PM, and stator core loss. For LSPMMs, eddy current loss of the PM and rotor core loss change very little when the magnetic flux density changes [17,18]. Therefore, stator core loss is mainly considered when the magnetic load is changing, and the copper loss of the stator winding is mainly considered when the current density is changing [19,20]. These two losses will affect the efficiency and the temperature characteristics of the motor [21]. In addition, for LSPMMs, due to the different heat dissipation characteristics of the core and winding, even at the same efficiency, different distributions of core loss and winding loss will result in different temperature distributions. However, in the existing literature, the electromagnetic properties are usually designed and optimized for maximum efficiency [22]. When the efficiency is high, the temperature performance of the motor may not be the optimal due to different core loss and winding loss distributions. The temperature characteristics of some LSPMMs are also analyzed based on different cooling schemes [11,23,24]. In these analyses, the effects of electromagnetic design parameters, especially the magnetic load and current density on the temperature, are not analyzed and summarized, which makes it difficult for designers to select optimal electromagnetic parameters to achieve better temperature performance. Therefore, comparative analysis of temperature characteristics considering magnetic load and current density should be studied and summarized for outer rotor LSPMMs.

In this paper, the temperature characteristics under different magnetic loads and stator current densities are compared and a final scheme is obtained, which has a lower temperature distribution than the initial scheme. In Section 2, the motor parameters and structure of the initial scheme are determined. In Section 3, the electromagnetic and temperature properties of the initial scheme are obtained through 2D-FEA using Motor-CAD and Ansys Maxwell software. In Section 4, by comparing the temperature and loss under different magnetic loads and different current densities, the effects of magnetic load and current density on temperature are revealed. Then, four different schemes are proposed, and the loss and temperature characteristics of these four schemes under rated load are compared. In Section 5, a final scheme is proposed and its temperature and loss characteristics are compared with the initial scheme, verifying the validity of our conclusions. In Section 6, a prototype is built and tested to verify the feasibility of our conclusions. For LSPMM design, the conclusions summarized in this paper can truly help researchers to choose a better scheme to realize better motor temperature performance.

2. Motor Parameters and Structure of Initial Scheme

A 200 kW 56 rpm motor is taken as the research object. The motor structure and parameters of initial scheme are provided in Figure 1 and Table 1. Considering the low

speed, the motor adopts an outer rotor structure to meet the large torque [13]. In addition, the surface-mounted permanent magnet (PM) structure is applied, because the surface-mounted permanent magnet structure has less flux leakage and simpler structure than the interior permanent magnet structure [17]. In order to achieve a better cooling effect, the structure of axial spiral water cooling is adopted.

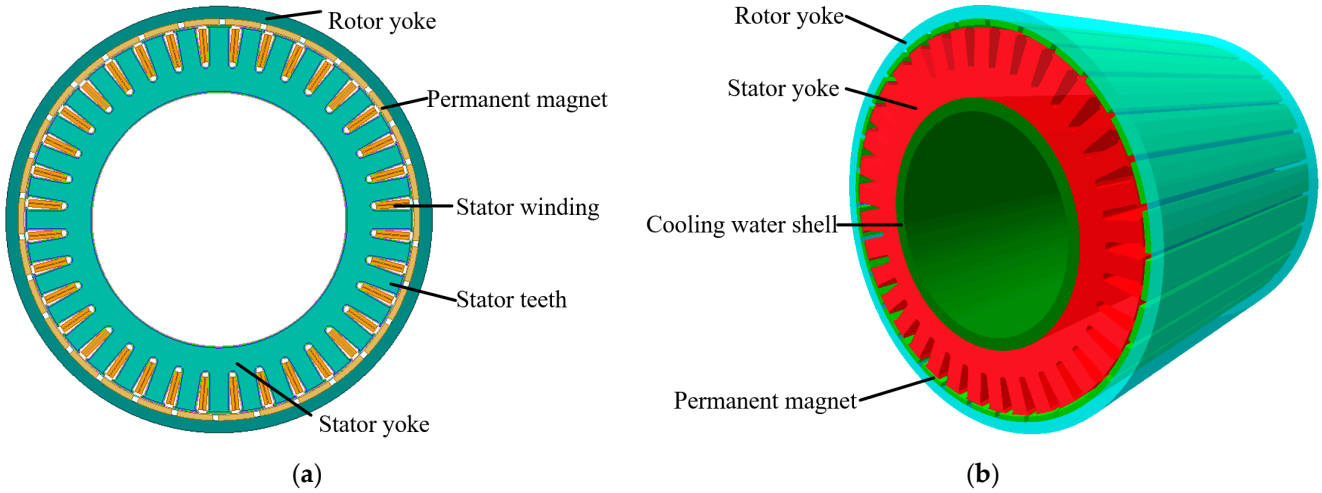

Figure 1. Motor structure: (**a**) planar structure; (**b**) 3D structure.

Table 1. The parameters of initial scheme.

Parameters	Values
Rated power (kW)	200
Rated speed (rpm)	56
Rated voltage (V)	380
Stator outer diameter (mm)	880
Core length (mm)	917
Pole number	30
Stator slot number	36
Air-gap length (mm)	3
Current density (A/mm^2)	4

3. Electromagnetic and Temperature Characteristics of the Initial Scheme

On the basis of the initial scheme, the motor model is established using Ansys Maxwell software. Zero current is set during no-load analysis, and a three-phase rated current is set during load simulation. After the boundary conditions are set, the electromagnetic properties under no-load state and rated load are calculated and analyzed by 2D-FEA.

The magnetic flux density distributions of the motor under no-load state and rated load conditions are shown in Figure 2. In these two states, a small part of the stator teeth region is saturated in magnetic flux density, but the magnetic flux density of the other part behaves well.

Figure 3 shows the variation of radial air-gap magnetic flux density with mechanical angle waveform and Fourier transform results under no-load state. As shown, the peak value of the radial air-gap magnetic flux density is 1.14 T. In addition, the 5th and 7th harmonic amplitudes of the radial air-gap flux density are small compared to the fundamental amplitude of the radial air-gap flux density. The waveform and Fourier transform result of line-to-line back electromotive force (back-EMF) under no-load state are shown in Figure 4. The amplitude of the no-load back-EMF line-to-line voltage is about 520 V, and its image is very smooth.

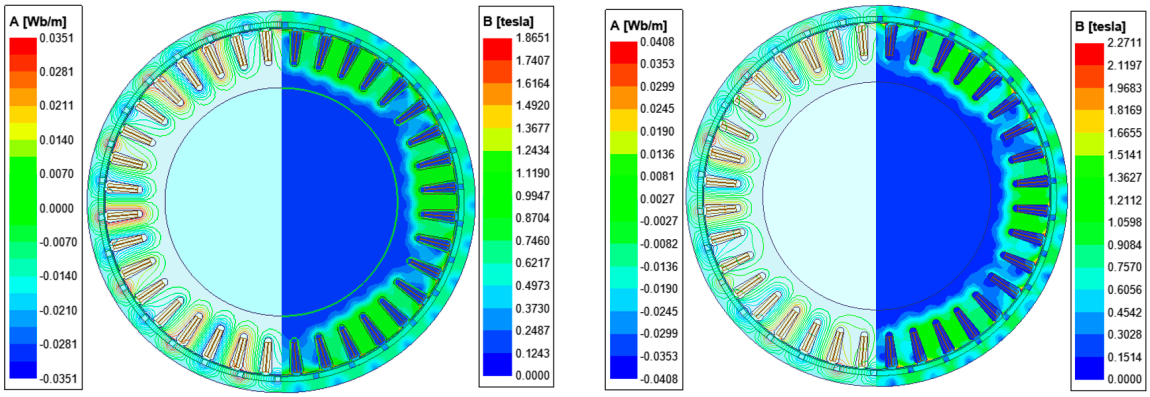

(**a**) (**b**)

Figure 2. Magnetic flux density distributions under no-load state and rated load: (**a**) no-load state; (**b**) rated load.

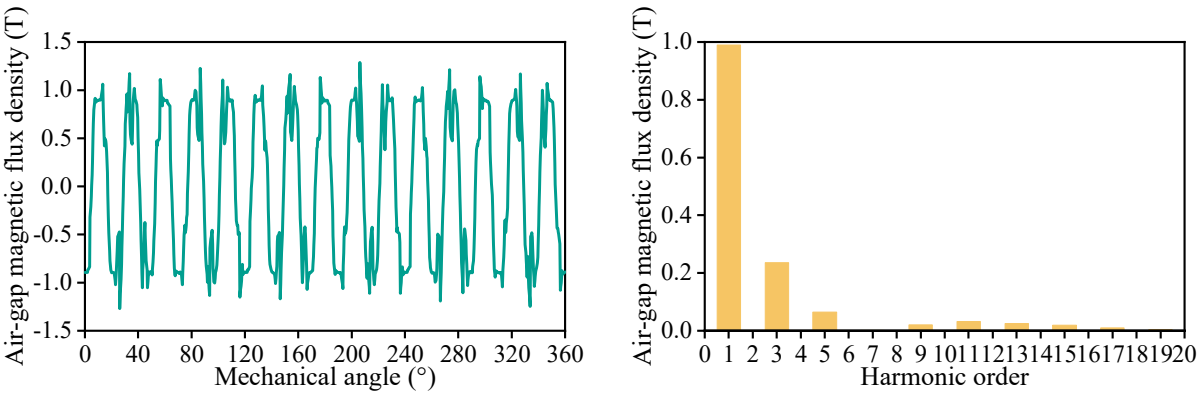

(**a**) (**b**)

Figure 3. Radial air-gap magnetic flux density and Fourier transform results under no-load state: (**a**) radial air-gap magnetic flux density; (**b**) Fourier transform.

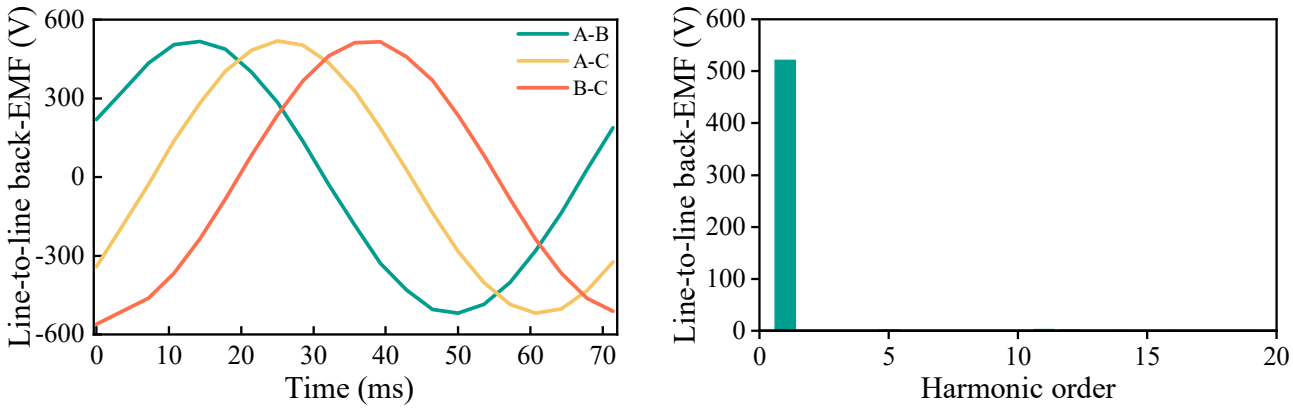

(**a**) (**b**)

Figure 4. Line-to-line back-EMF and Fourier transform results: (**a**) line-to-line back-EMF waveform; (**b**) Fourier transform.

Figure 5 shows the cogging torque and the output torque under rated load. As shown in the figure, the output torque under rated load is 34,700 N·m, and the ripple of the output torque is only 2%. The core loss and eddy current loss of PM under rated load are shown in

Figure 6. After entering the steady state, the average values of core loss and eddy current loss of the PM are 3748 W and 667 W, respectively. In addition, the copper loss is 12,430 W.

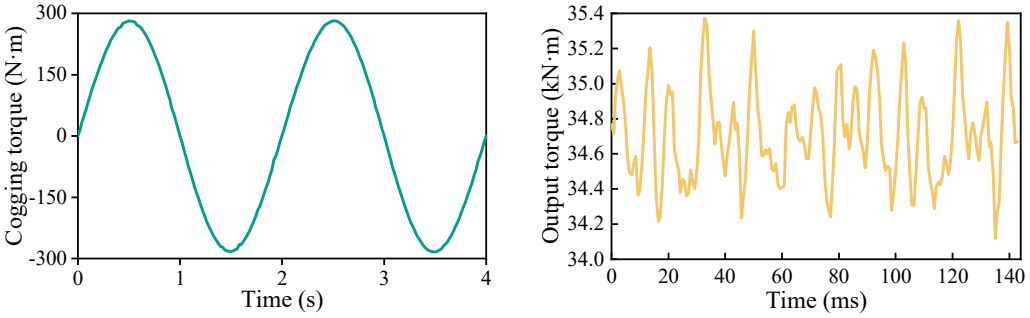

(**a**) (**b**)

Figure 5. Cogging torque and output torque under rated load: (**a**) cogging torque; (**b**) output torque.

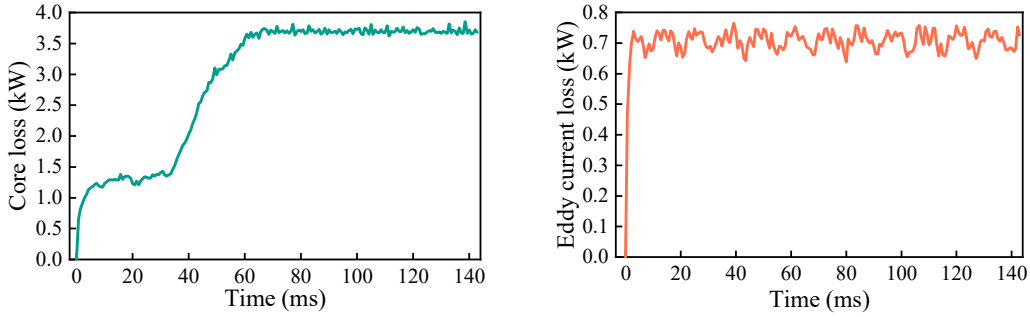

(**a**) (**b**)

Figure 6. (**a**) Core loss and (**b**) eddy current loss of the PM under rated load.

In order to obtain the temperature characteristics of the initial scheme, an FEA of temperature is conducted using Motor-CAD software. The axial spiral water cooling, inlet velocity, and inlet temperature are also set in the FEA. In addition, in order to consider the influence of the air-gap and rotational speed on the heat transfer characteristics of the motor, the rotational speed of the motor is set to 56 rpm, the length of the air-gap is set to 3 mm in the FEA. The temperature distribution of the initial scheme is shown in Figure 7. The lowest temperature occurs at the rotor yoke, which is 69.4 °C. The highest temperature occurs at the stator winding caused by the large copper loss of winding, which is 122.7 °C. The temperature of the stator teeth is higher than that of the stator yoke.

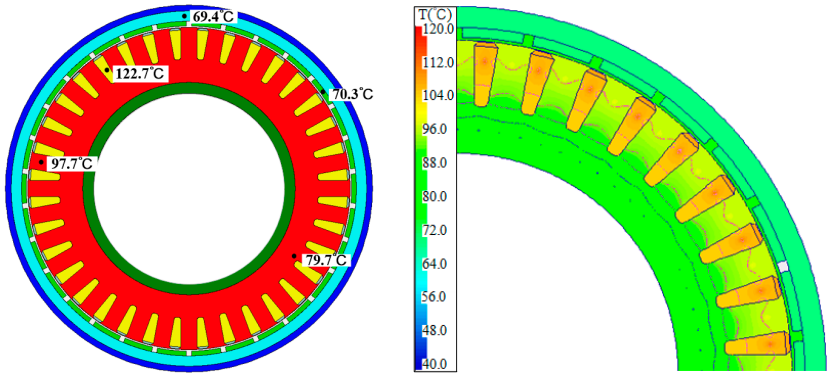

(**a**) (**b**)

Figure 7. Temperature distribution of motor under rated load: (**a**) whole temperature distribution; (**b**) partial temperature distribution.

4. Influence of Magnetic Load and Current Density on Temperature

4.1. Influence of Magnetic Load on Motor Temperature

This section studies the effect of magnetic load on temperature, and the stator core loss is used to reflect the change in magnetic load. The relationship between stator core loss and stator magnetic flux density can be obtained by the following equations [19,20]:

$$P_{Fe\_yoke} = C_{Fej} f^{1.3} B_j{}^2 G_j \quad (1)$$

$$P_{Fe\_teeth} = C_{Fei} f^{1.3} B_i{}^2 G_i \quad (2)$$

where P_{Fe_yoke} is the core loss of stator yoke, C_{Fej} is the core loss coefficient of stator yoke, G_j is the weight of the stator yoke, B_j is the magnetic flux density of the stator yoke, P_{Fe_teeth} is the core loss of stator teeth, C_{Fei} is the core loss coefficient of stator teeth,G_i is the weight of the stator teeth, B_i is the magnetic flux density of the stator teeth, f is the frequency of the magnetic field.

From Equations (1) and (2), the stator core losses under different stator magnetic flux densities are obtained, and the results are shown in Figure 8. The stator core loss increases from 2724 W to 4843 W, and the stator magnetic flux density increases from 1.2 T to 1.6 T.

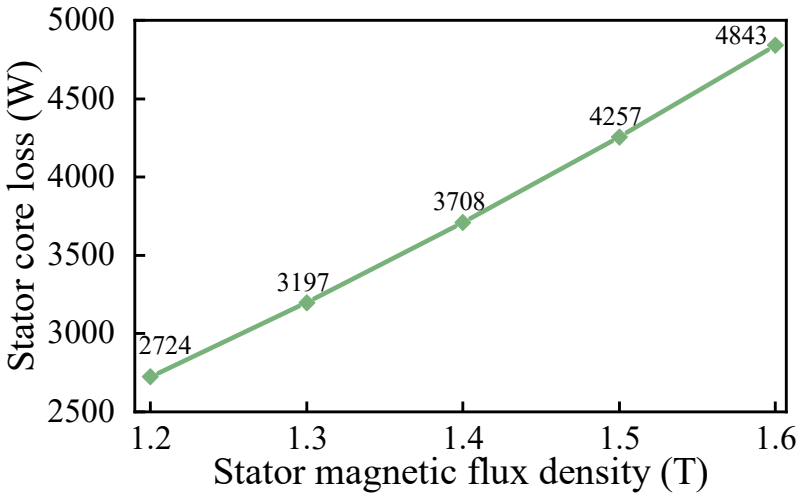

Figure 8. Stator core loss under different stator magnetic flux density.

The temperature distribution and comparison of the motor under different stator magnetic flux densities are shown in Figures 9 and 10. As shown in Figure 9, the highest temperature still occurs at the winding, and the lowest temperature appears at the rotor yoke. When the stator magnetic flux density increases from 1.2 T to 1.6 T, the temperature of each part increases. Among them, the temperature rise at the stator winding is the highest, which is only 9 °C. The temperature rise at PM is the smallest, which is 2.7 °C. Therefore, changes in magnetic flux density have a mild effect on temperature.

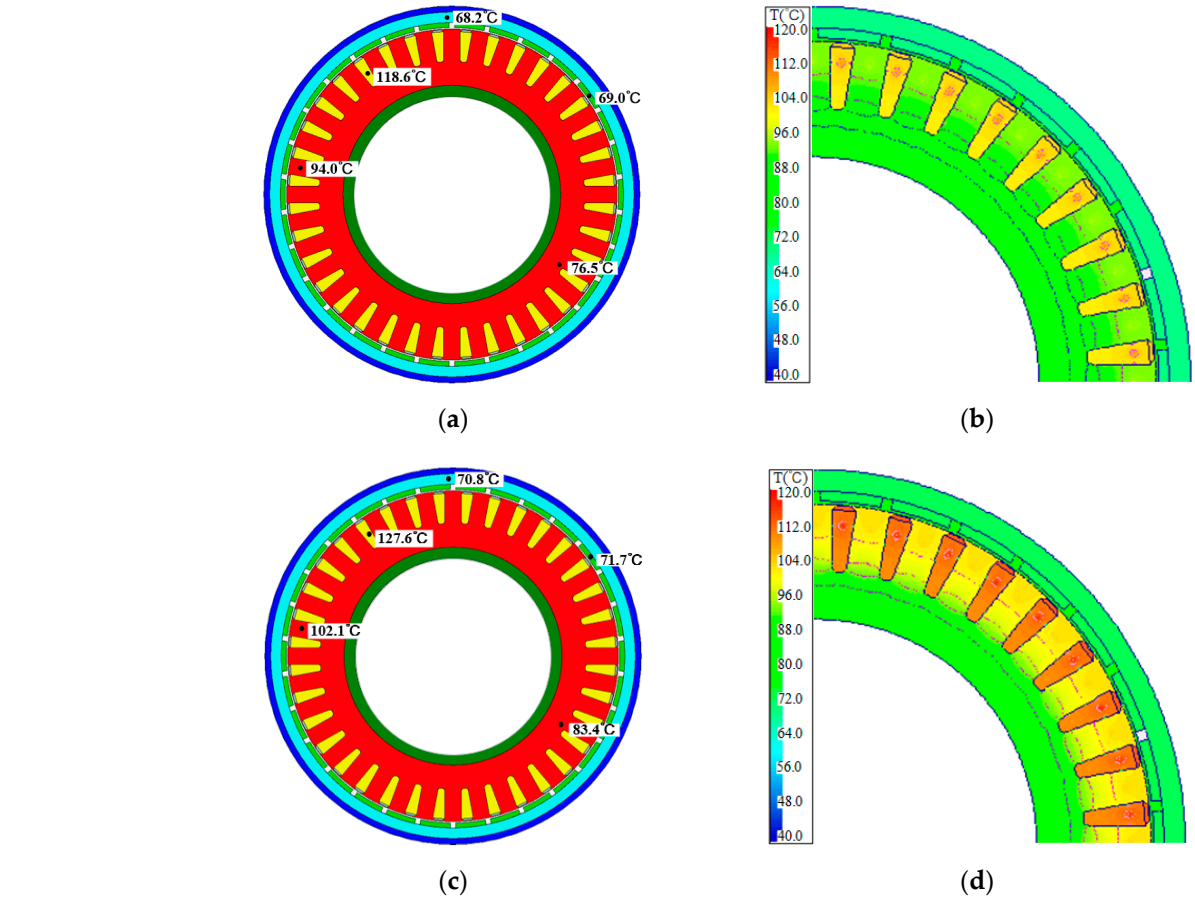

Figure 9. Temperature distributions under 1.2 T and 1.6 T: (**a**) whole temperature distribution under 1.2 T; (**b**) partial temperature distribution under 1.2 T; (**c**) whole temperature distribution under 1.6 T; (**d**) partial temperature distribution under 1.6 T.

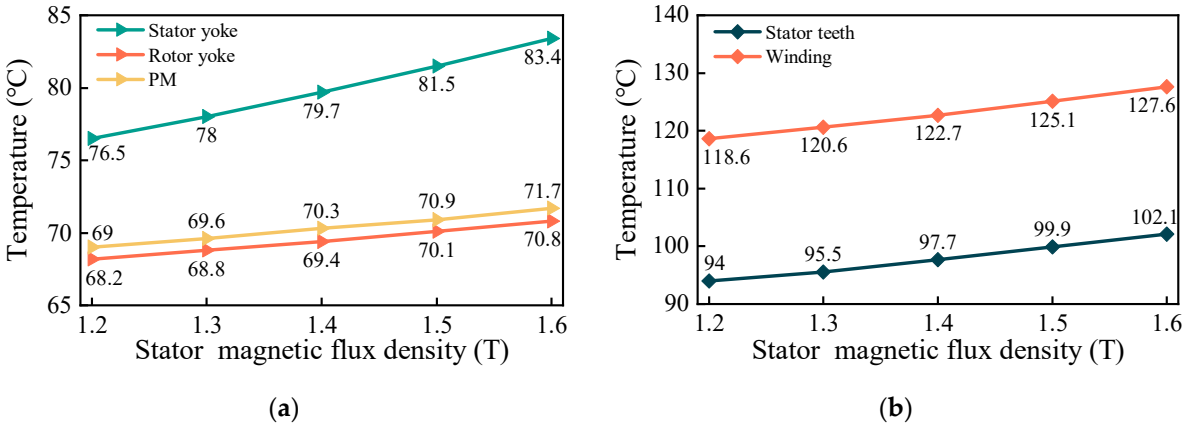

Figure 10. Temperature comparisons under different stator magnetic flux densities: (**a**) temperature comparisons of stator yoke, rotor yoke, and PM; (**b**) temperature comparisons of stator teeth and winding.

4.2. Influence of Current Density on Motor Temperature

The effect of current density on temperature is explored in this section. The relationship between copper loss of winding and current density can be obtained using the following equations [17]:

$$P_{Cu} = m{I_{ph}}^2 R_{ph} \quad (3)$$

$$R_{hf} = \rho \frac{l}{A_o} \tag{4}$$

$$J = \frac{I_{ph}}{A_o} \tag{5}$$

$$P_{Cu} = mplI_{ph}J \tag{6}$$

where P_{Cu} is the copper loss of the valid part, m is the phase number, I_{ph} is the phase current, R_{ph} is the effective partial resistance of each phase conductor, A_o is the conductor's effective cross-sectional area, l is the core length, ρ is the resistivity of conductor materials, J is the current density.

The copper losses at different current densities are obtained via Equation (6), as shown in Figure 11. From the figure, it can be seen that the copper loss of winding increases by 12,127 W when the current density increases from 2 A/mm^2 to 6 A/mm^2.

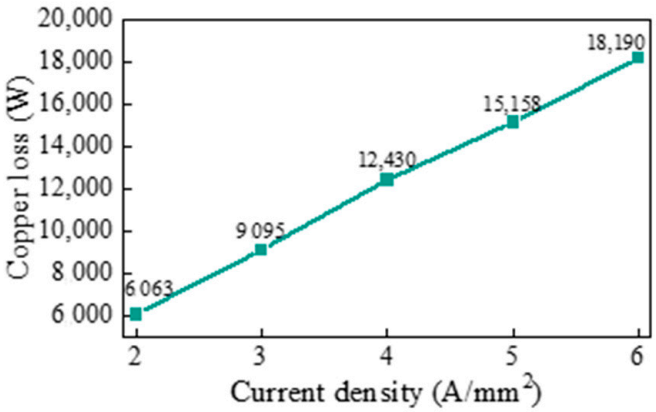

Figure 11. Copper loss under different current densities.

Figures 12 and 13 show the temperature distributions and comparisons, respectively, at different current densities. As shown, when the current density is 6 A/mm^2, the temperature of each part of the motor is the highest, and the temperature of the stator winding is 160.8 °C. Compared with the current density of 2 A/mm^2, the temperature of the stator winding at the current density of 6 A/mm^2 increased by 80.1 °C. Therefore, the temperature is greatly affected by the current density.

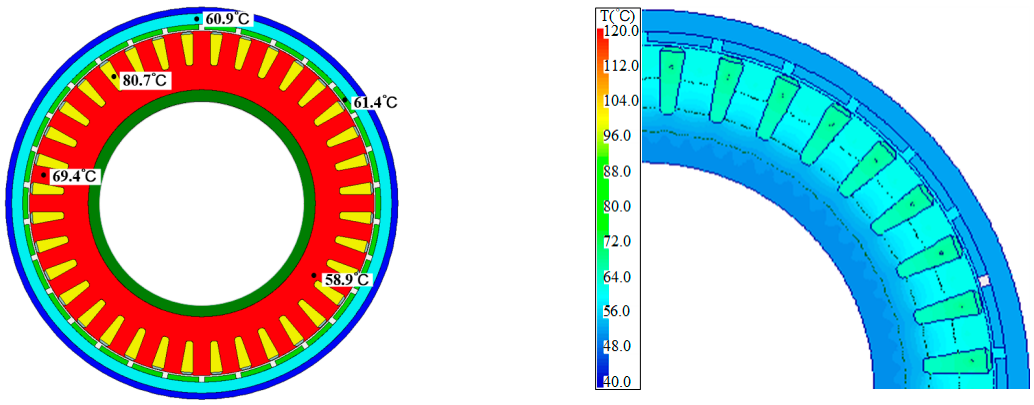

(**a**) (**b**)

Figure 12. *Cont.*

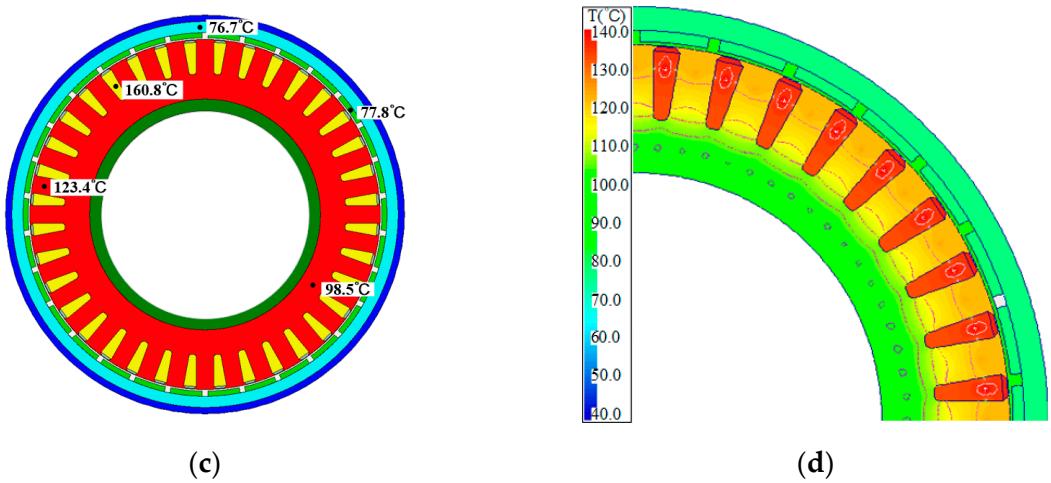

Figure 12. Temperature distributions under 2 A/mm^2 and 6 A/mm^2: (**a**) whole temperature distribution under 2 A/mm^2; (**b**) partial temperature distribution under 2 A/mm^2; (**c**) whole temperature distribution under 6 A/mm^2; (**d**) partial temperature distribution under 6 A/mm^2.

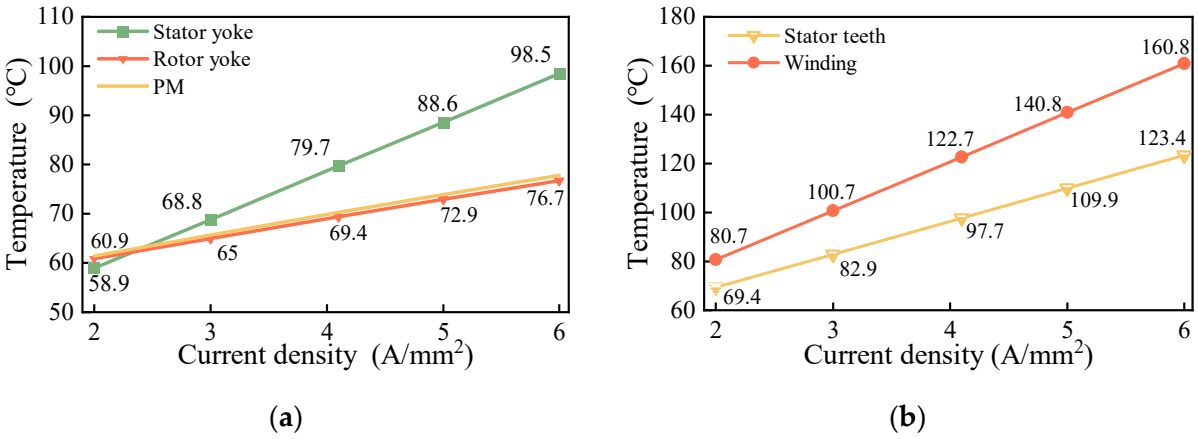

Figure 13. Temperature comparisons under different current densities: (**a**) temperature comparisons of rotor yoke, stator yoke, and PM; (**b**) temperature comparisons of stator teeth and winding.

4.3. Combined Effect of Magnetic Load and Current Density on Temperature

Four schemes are proposed to explore the combined effects of magnetic load and current density on temperature under rated load. Among them, the current density of Case 1 and Case 2 remains unchanged, while the magnetic load is changed. The air-gap magnetic flux densities of Case 3 and Case 4 are unchanged, and the current densities are changed. In addition, the back-EMF, stator outer diameter, and slot fill rate of the four schemes also remain unchanged.

The parameters of the four schemes are shown in Table 2. As shown, the permanent magnet thickness and pole embrace of Case 1 are increased to achieve higher magnetic load, while the pole embrace of Case 2 is decreased to reduce the magnetic load. Furthermore, to maintain the same back-EMF, the core length of Case 1 is shortened, while the core length of Case 2 is increased. For Case 3 and Case 4, in order to achieve higher current density, the parallel winding number is reduced in Case 3, and in Case 4, the parallel winding number is increased to reduce the current density. To guarantee the same slot fill rate of 75%, the slot area of Case 3 is reduced and the slot area of Case 4 is increased.

Table 2. The parameters of four schemes.

Design Scheme	Case 1	Case 2	Case 3	Case 4
Core length (mm)	842	992	917	917
PM thickness (mm)	19.1	13	13	13
Pole embrace	0.9	0.7	0.85	0.85
Conductor parallel winding number	18	18	14	24
Slot width (mm)	23	23	23	23
Slot height (mm)	85	85	68	112
Air-gap magnetic flux density (T)	0.92	0.84	0.84	0.84
Stator teeth magnetic flux density (T)	1.53	1.2	1.4	1.5
Stator yoke magnetic flux density (T)	0.59	0.44	0.42	0.97
Current density (A/mm^2)	4	4	5.2	3

Figure 14 shows the magnetic flux density distribution for the four schemes. From the figure, the air-gap flux density and stator teeth flux density of Case 1 are the largest, and its air-gap magnetic flux density and stator teeth magnetic flux density are 0.92 T and 1.53 T, respectively. The magnetic load in Case 2 is the smallest, and its air-gap magnetic flux density and stator teeth magnetic flux density are 0.84 T and 1.2 T. Although the air-gap magnetic flux densities of Cases 2, 3, and 4 are the same, the stator magnetic flux densities of Case 3 and Case 4 are different due to the change in the slot area. The stator teeth magnetic flux density of Case 3 is 1.34 T, and the stator teeth magnetic flux density of Case 4 is 1.5 T, which is close to the maximum of the stator teeth magnetic flux density. In addition, the magnetic flux density of the stator yoke of Case 4 is the largest, because the increase in the slot depth reduces the area of the stator yoke part.

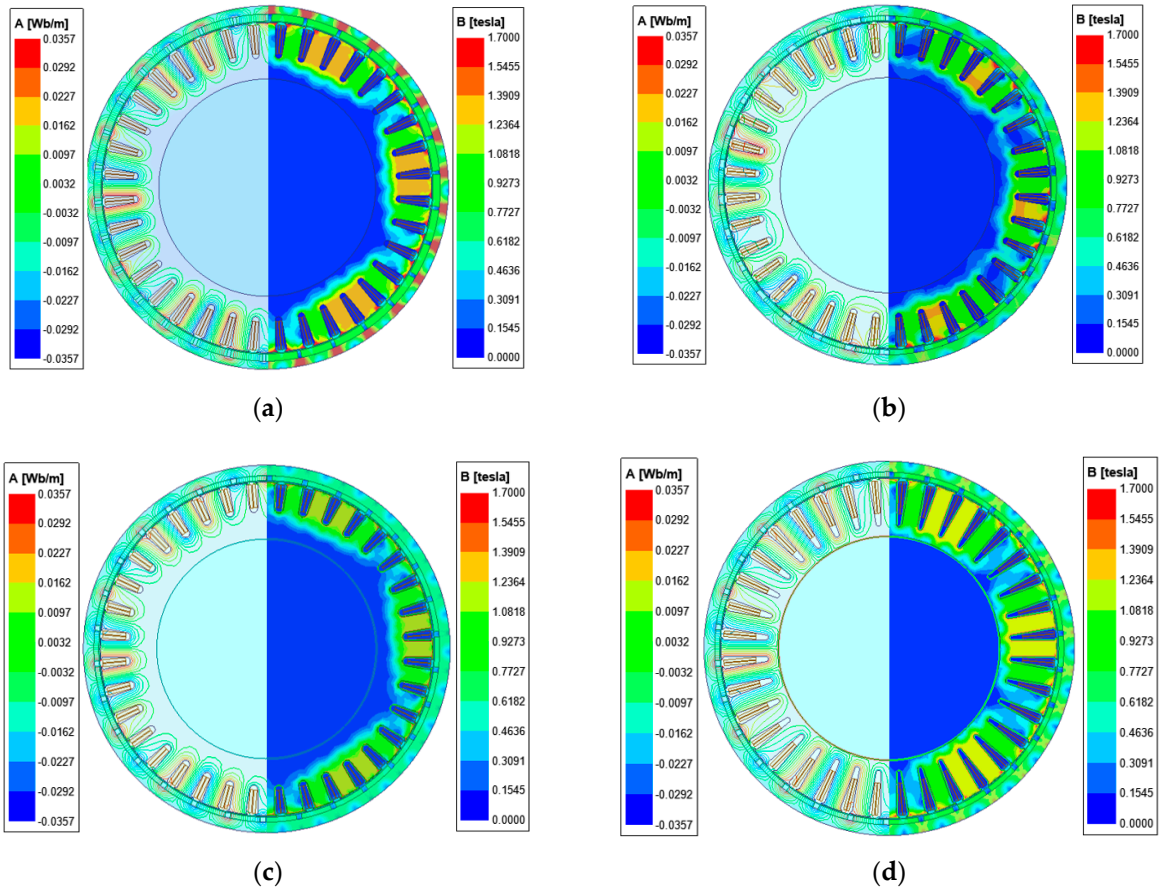

Figure 14. Magnetic flux density distributions under four schemes: (**a**) Case 1; (**b**) Case 2; (**c**) Case 3; (**d**) Case 4.

After 2D-FEA simulation using Ansys Maxwell software, the stator core loss, rotor core loss, eddy current loss of the PM, and copper loss under rated load are obtained, as shown in Figure 15. It can be seen that Case 4 has the largest stator core loss, which is 4548 W. This is because, among the four schemes, Case 4 has the same maximum stator teeth magnetic flux density as Case 1, and the core length of Case 4 is longer than that of Case 1. The stator core loss of Case 3 is the smallest, which is 2978 W, because although the stator magnetic flux density of Case 3 is larger than that of Case 2 (which has the smallest stator magnetic flux density), the core length of Case 3 is shorter than that of Case 2. In addition, the stator core losses for Case 1 and Case 2 are 3923 W and 3284 W, respectively. The stator core loss of Case 1 is larger than that of Case 2; this is because although the core length of Case 1 is shorter than Case 2, the magnetic load is larger. For the rotor core loss, the maximum value is 58 W in Case 2. For eddy current loss of the PM, Case 3 has the largest eddy current loss at 700 W. The smallest eddy current loss of the PM is 527 W, which occurs in Case 2. In addition, the maximum copper loss is 16,005 W, which appears in Case 3; this is because Case 3 has the highest current density. The copper loss of Case 4 is the smallest, at 9407 W, because the current density of Case 4 is the smallest. For Case 1 and Case 2, since the core length of Case 2 is longer than that of Case 1, and the current densities of the two cases are the same, the copper loss of Case 2 is larger.

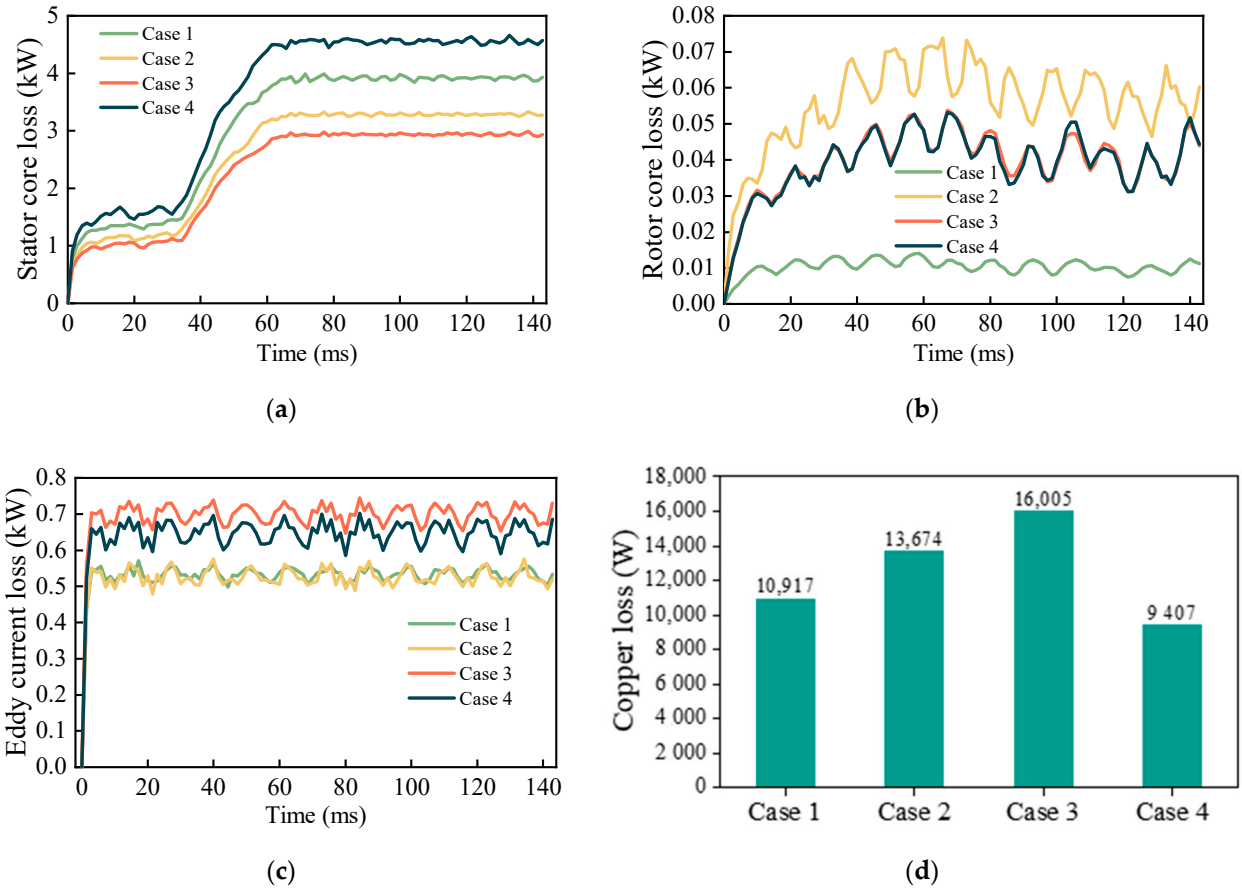

Figure 15. Loss of four schemes under rated load: (**a**) stator core loss; (**b**) rotor core loss; (**c**) eddy current loss of the PM; (**d**) copper loss.

Figures 16 and 17 show the temperature distribution and comparison under the four schemes. From the figure, the temperature of each part of Case 3 is the highest: temperature of the stator winding is 150 °C, and the temperature of PM is 75.6 °C. In contrast, Case 4 has the lowest temperature: the stator winding temperature is 102.2 °C, and the PM temperature is 66 °C. For Case 1 and Case 2, Case 1 (with the higher magnetic load) has the lower temperature. This is because compared with Case 2, although Case 1 has a larger

magnetic load, resulting in greater stator core loss, the reduction in copper loss due to the reduction in the core length is greater than the increase in stator core loss. Therefore, the increase in the magnetic load does not necessarily lead to an increase in the temperature, because the shortening of the core length may counteract this by reducing the temperature. In addition, among the four schemes, Case 4 has the smallest current density and copper loss, and has the largest stator magnetic flux density and stator core loss. Compared to the other schemes, the current density of Case 4 decreases, respectively, by 1 A/mm^2, 1 A/mm^2, and 2.2 A/mm^2, resulting in a reduction in copper loss by 1510 W, 4267 W, and 6598 W, while the stator core loss increases by 625 W, 1264 W, and 1610 W. Furthermore, compared with the other three schemes, the stator winding temperature of Case 4 is reduced by 18.1 °C, 20.7 °C, and 48.8 °C, respectively. Obviously, with the further decrease in the current density, although the stator core loss increases, the copper loss due to the changes in current density decreases further, and the temperature still drops significantly. Therefore, for LSPMMs, the motor temperature is significantly affected by current density.

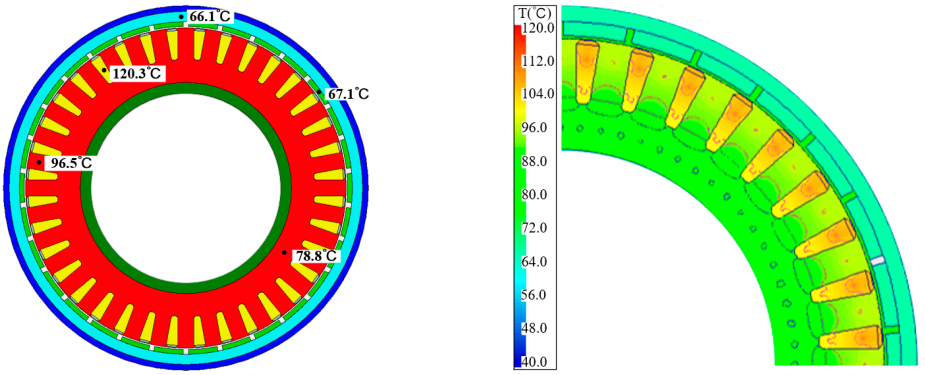

(**a**)

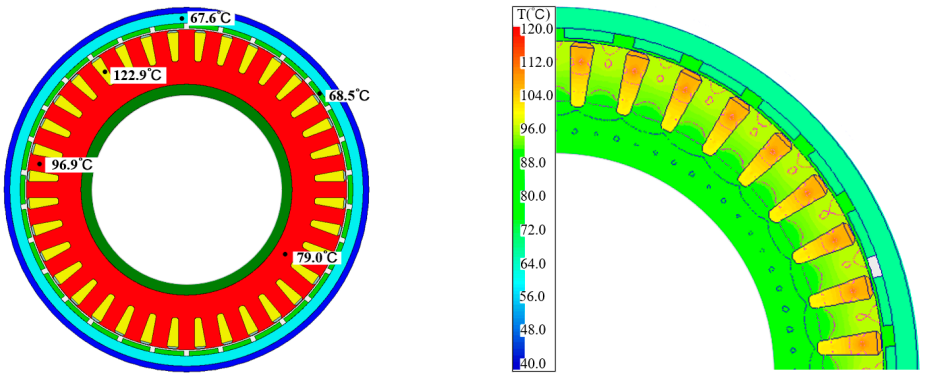

(**b**)

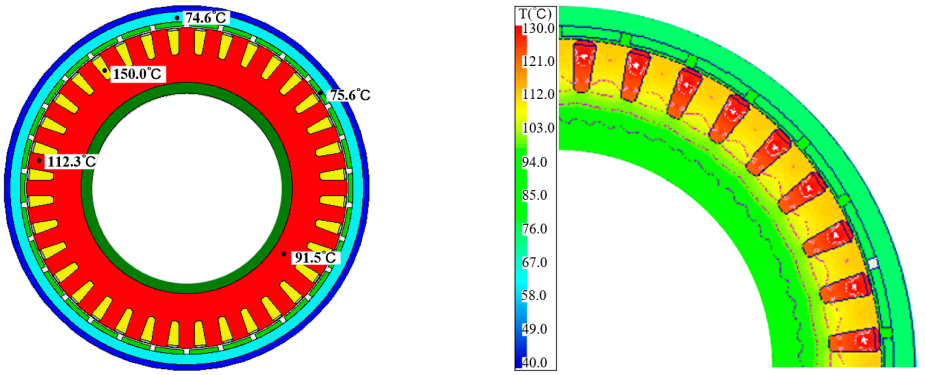

(**c**)

Figure 16. *Cont.*

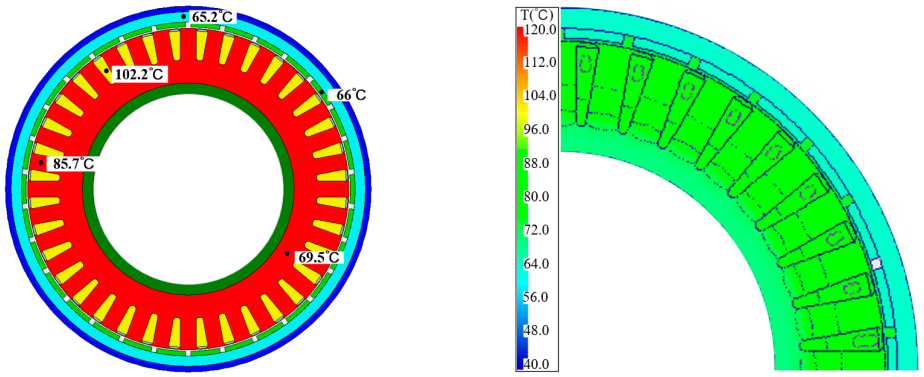

(**d**)

Figure 16. Temperature distribution under four design schemes: (**a**) Case 1; (**b**) Case 2; (**c**) Case 3; (**d**) Case 4.

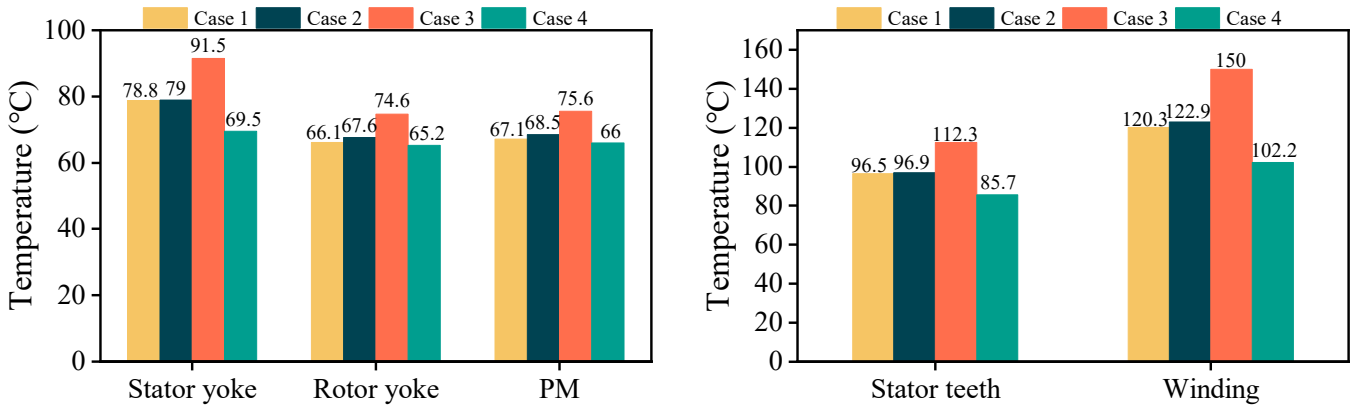

(**a**) (**b**)

Figure 17. The temperature comparisons of four schemes: (**a**) temperature comparisons of stator yoke, rotor yoke, and PM; (**b**) temperature comparisons of stator teeth and winding.

5. Final Scheme

Based on the above analysis, a final scheme is determined. Compared with Case 4, which had the lowest temperature, the magnetic load of the final scheme is further increased to achieve lower temperature rise and smaller motor volume. Furthermore, the final scheme has higher magnetic load and lower current density compared to the initial scheme.

The parameter comparison between the final scheme and the initial scheme is shown in Table 3. The PM thickness and pole embrace of the final scheme are increased to obtain higher magnetic load, and the parallel winding number is increased to obtain a smaller current density. In addition, the core length of the final scheme is shortened to ensure the same back-EMF. In order to realize the same slot fill rate, the slot area of final scheme is also reduced. Moreover, in final and initial schemes, the back-EMF, the stator outer diameter, and the slot fill rate remain unchanged.

Figure 18 shows the magnetic flux density distribution of the final scheme obtained by 2D-FEA using Ansys Maxwell software. As shown, the magnetic flux densities of the stator teeth and yoke are 1.6 T and 0.97 T, respectively, and the air-gap magnetic flux density is 0.88 T; these values are increased compared to the initial scheme. Although the magnetic load of the final scheme has increased significantly, the stator magnetic flux density still does not exceed 1.8 T, and does not reach saturation.

Table 3. The parameters comparisons of the final and initial schemes.

Design Scheme	Final Scheme	Initial Scheme
Core length (mm)	874	917
PM thickness (mm)	16	13
Pole embrace	0.9	0.85
Conductor parallel winding number	24	18
Slot width (mm)	23	23
Slot height (mm)	112	85
Air-gap magnetic flux density (T)	0.88	0.84
Stator teeth magnetic flux density (T)	1.6	1.4
Stator yoke magnetic flux density (T)	0.97	0.53
Current density (A/mm^2)	3	4

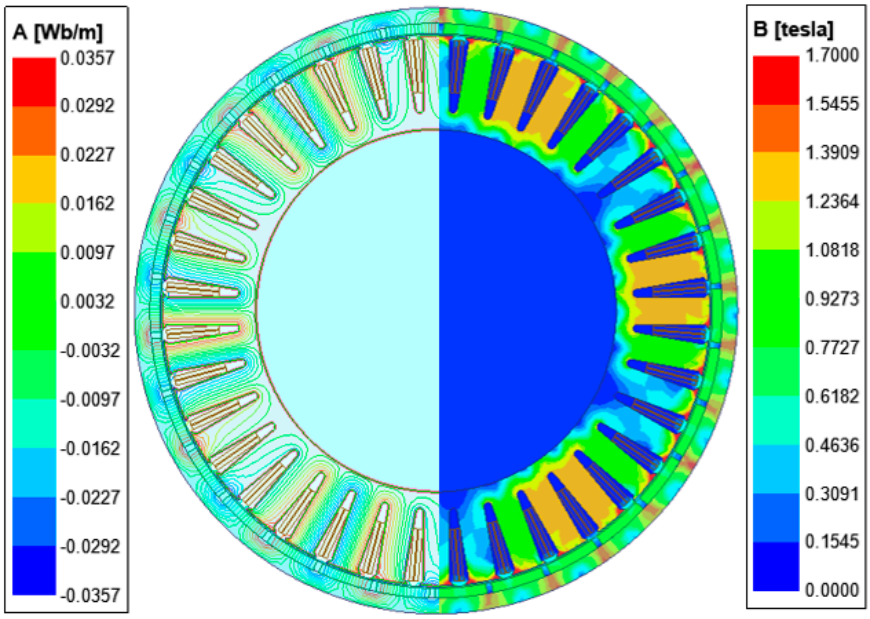

Figure 18. The magnetic flux density distribution of the final scheme.

The core loss and eddy current loss of the PM in the final scheme at rated load are shown in Figure 19. After entering the steady state, the average core loss of the final scheme is 4870 W, the average eddy current loss of the PM is 602 W, and the average copper loss is 8655 W. Compared with the initial scheme, the core loss of the final scheme increases by 1122 W, caused by the increase in magnetic load. In addition, due to the reduction in current density and core length of the final scheme, the copper loss has dropped by 3775 W. The eddy current loss of the PM has not changed substantially in two schemes.

Figures 20 and 21 show the temperature distribution and comparison at rated load for the final and initial schemes. Compared with the initial scheme, since the copper loss of final scheme decreases more than the stator core loss increases, the temperature of each part of the motor has dropped considerably in the final scheme. The temperature of the stator winding part has dropped the most, reaching 21 °C. Therefore, in the design of outer rotor LSPMMs, lower current density and higher magnetic load can effectively improve temperature characteristics and reduce the size of the motor.

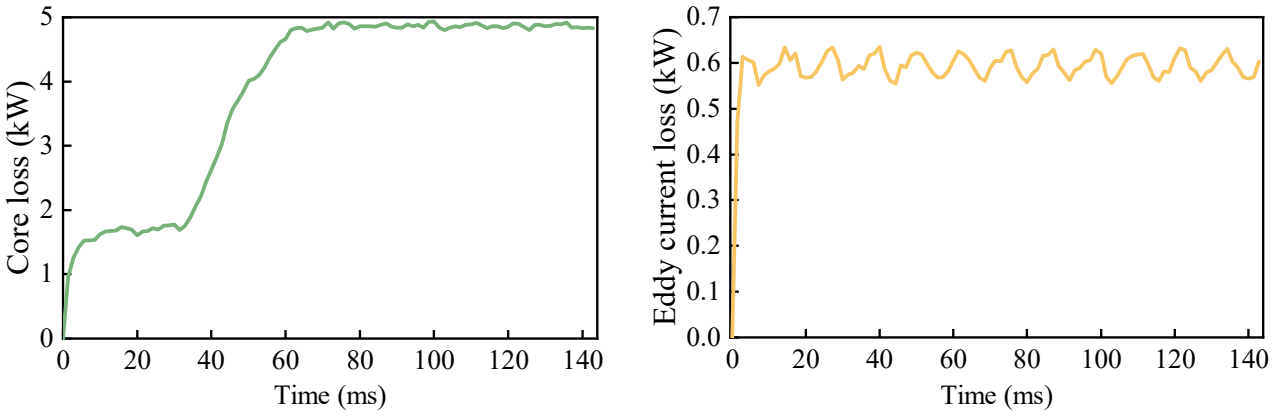

Figure 19. The core loss and eddy current loss of PM in final scheme: (**a**) core loss; (**b**) eddy current loss of the PM.

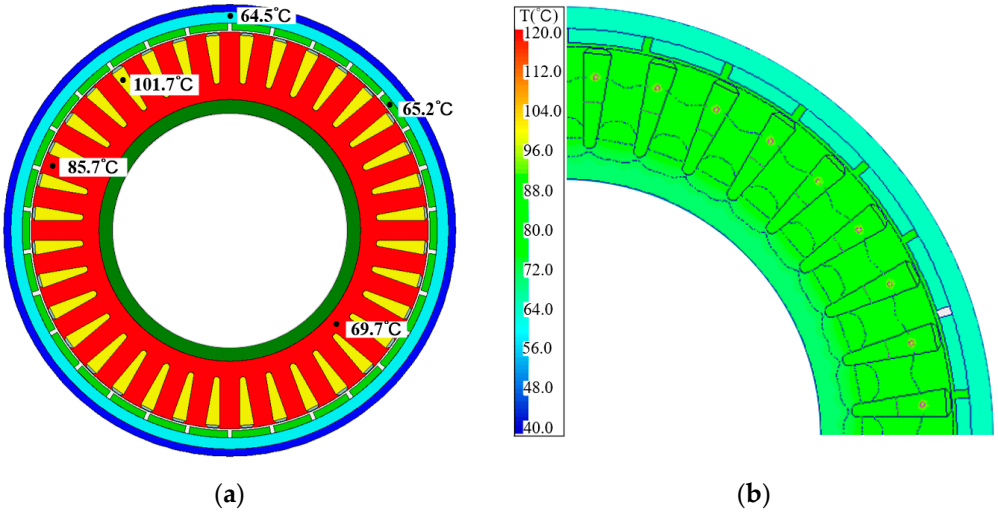

Figure 20. Whole and partial temperature distribution of final scheme: (**a**) whole temperature distribution; (**b**) partial temperature distribution.

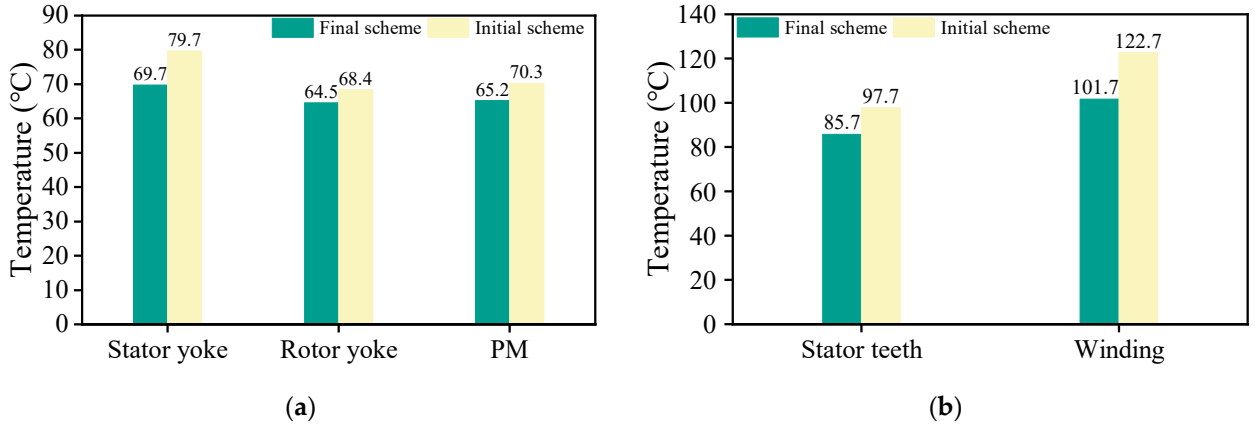

Figure 21. The temperature comparison between final scheme and initial scheme: (**a**) temperature comparisons for stator yoke, rotor yoke, and PM; (**b**) temperature comparisons for stator teeth and winding.

6. Experimental Test

A 22 kW 56 rpm prototype is made to verify the feasibility of the previous conclusions. The prototype is shown in Figure 22. The prototype adopts an outer rotor structure and surface-mounted permanent magnets, and double-layer windings are applied.

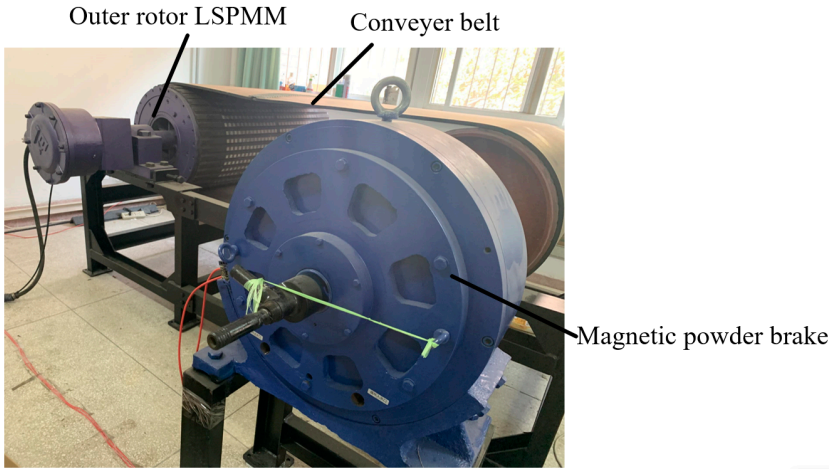

Figure 22. Prototype.

The winding temperature is measured by Pt100 resistance temperature detectors in the end windings. The efficiency of the prototype and the stator winding temperature are obtained after the prototype is run. At rated load, the measured efficiency of the prototype is 94.2%, which is slightly lower than the calculated value. In addition, the stator winding temperature of the prototype is 109 °C, which is 3 °C higher than the calculated value. Furthermore, the continuous normal operation and good temperature performance of the prototype verify the feasibility of our conclusions.

7. Conclusions

In this paper, the temperature and loss characteristics under different magnetic loads and current densities are compared and investigated. The comprehensive effects of magnetic load and current density on temperature are further revealed. On the basis of the conclusions obtained, the temperature characteristics of the final scheme and the prototype are analyzed to verify the validity and feasibility of our conclusions. The key points are summarized as follows:

1. When the stator magnetic flux density increases from 1.2 T to 1.6 T, although the temperature of each part of the motor increases, the highest temperature rise is only 9 °C, which appears at the stator winding. In addition, the temperature of the PM only increases by 2.7 °C. Therefore, an increase in the magnetic load does not cause a significant increase in the temperature for LSPMMs.
2. Case 1 and Case 2 have the same current density. However, compared with Case 2, the core loss of Case 1 increases by 639 W due to the higher magnetic load. In addition, in order to ensure the same back-EMF, the core length of Case 1 is shortened while increasing the magnetic load, resulting in lower copper loss of Case 1. The copper loss of Case 1 is reduced by 2757 W compared with Case 2, which is about five times the increase in stator core loss. Therefore, Case 1, with a higher magnetic load, has a lower temperature under rated load compared with Case 2. The winding and PM temperatures of Case 1 are 120.3 °C and 78.8 °C, respectively, and the temperature of the corresponding parts of Case 2 are 122.9 °C and 68.5 °C. Thus, for LSPMM design, an increase in the magnetic load may not lead to an increase in the temperature, because the core length will also be shortened, resulting in lower copper loss and the possibility of a temperature drop.

3. Among the four schemes, Case 4 has the smallest current density, but has the largest stator magnetic flux density and stator core loss. Compared with the other three schemes, the current density of Case 4 is reduced by 1 A/mm^2, 1 A/mm^2, 2.3 A/mm^2 in turn, resulting in a reduction in copper loss by 1510 W, 4267 W, and 6598 W, while the stator core loss increases by 625 W, 1264 W, and 1610 W, respectively. However, the temperature of Case 4 is the lowest. Compared with the other three cases, the stator winding temperature of Case 4 drops by 18.1 °C, 20.7 °C, and 48.8 °C. It can be summarized that although the stator core loss keeps increasing, the copper loss due to the decrease in current density decreases more sharply; thus, the temperature still decreases. Therefore, for LSPMMs, the motor temperature is significantly affected by current density.
4. After comparing the final scheme with the initial scheme, the final scheme with higher magnetic flux density and lower current density has a lower temperature. The stator winding temperature of the final scheme is 101.7 °C, and the stator winding temperature decreases by 21 °C compared to the initial scheme. In addition, the temperature performance of the manufactured prototype is also very good, and the error between the measured and calculated results of the temperature is only 2%. Therefore, in the design of outer rotor LSPMMs, lower current density and higher magnetic load can indeed lead to better temperature performance.

Author Contributions: Conceptualization, G.D. and Q.Z. (Qixun Zhou); Data curation, G.D. and Q.Z. (Qizheng Zhang); Formal analysis, Q.Z. (Qizheng Zhang); Funding acquisition, G.D.; Investigation, G.D. and Q.Z. (Qizheng Zhang); Methodology, G.D. and Q.Z. (Qizheng Zhang); Project administration, G.D.; Resources, G.D.; Software, Q.Z. (Qizheng Zhang); Supervision, Q.Z. (Qixun Zhou); Validation, G.D., Q.Z. (Qixun Zhou), T.P. and C.H.; Visualization, Q.Z. (Qizheng Zhang); Writing-original draft, Q.Z. (Qizheng Zhang); Writing-review & editing, G.D., Q.Z. (Qizheng Zhang), C.H. and T.P. All authors have read and agreed to the published version of the manuscript.

Funding: This research was funded by National Nature Science Foundation of China, grant number 52177056.

Institutional Review Board Statement: Not applicable.

Informed Consent Statement: Not applicable.

Data Availability Statement: Not applicable.

Conflicts of Interest: The authors declare no conflict of interest.

References

1. Crider, J.M.; Sudhoff, S.D. An Inner Rotor Flux-Modulated Permanent Magnet Synchronous Machine for Low-Speed High-Torque Applications. *IEEE Trans. Energy Convers.* **2015**, *30*, 1247–1254. [CrossRef]
2. Bao, X.H.; Li, J.W.; Yue, S.; Changjiang, W. Review and prospect of low-speed high-torque permanent magnet machines. *Trans. China Electrotech. Soc.* **2019**, *34*, 1148–1160.
3. Feng, L.S.; Yu, S.Y.; Zhang, F.G.; Shi, J.; Sun, Y.J. Study on Performance of Low-Speed High-Torque Permanent Magnet Synchronous Motor with Dynamic Eccentricity Rotor. *Energy Rep.* **2022**, *8*, 1421–1428. [CrossRef]
4. Xie, B.C.; Zhang, Y.; Wang, J.Q.; Liang, B.X.; Zhang, F.G. An Efficient Multidisciplinary Design Research for the Integrated Low Speed Permanent Magnet Motor System Based on Analytical and Numerical Hybrid Analysis. *Energy Rep.* **2022**, *8*, 199–208. [CrossRef]
5. Mohamed, Y.A.-R.I. A Newly Designed Instantaneous-Torque Control of Direct-Drive PMSM Servo Actuator with Improved Torque Estimation and Control Characteristics. *IEEE Trans. Ind. Electron.* **2007**, *54*, 2864–2873. [CrossRef]
6. Yan, B.; Wang, X.H.; Yang, Y.B. Starting Performance Improvement of Line-Start Permanent-Magnet Synchronous Motor Using Composite Solid Rotor. *IEEE Trans. Magn.* **2018**, *54*, 7400504. [CrossRef]
7. Rahman, K.M.; Schulz, S.E. Design of High-Efficiency and High-Torque-Density Switched Reluctance Motor for Vehicle Propulsion. *IEEE Trans. Ind. Appl.* **2002**, *38*, 1500–1507. [CrossRef]
8. Zhang, Y.J.; Sun, M.Y.; Ruan, J.J.; Huang, T. Ventilation Structure Improvement of Large Motors Using 3-D Multi-Physical Coupled-Field Finite-Element Analysis. In Proceedings of the 2012 Sixth International Conference on Electromagnetic Field Problems and Applications, Dalian, China, 19–21 June 2012; pp. 1–4.

9. Hong, J.; Park, S.; Hyun, D.; Kang, T.; Lee, S.B.; Kral, C.; Haumer, A. Detection and Classification of Rotor Demagnetization and Eccentricity Faults for PM Synchronous Motors. *IEEE Trans. Ind. Appl.* **2012**, *48*, 923–932. [CrossRef]
10. Zhou, G.H.; Xu, X.H.; Xiong, Y.; Zhang, L.C. Design and Analysis of Low-Speed High Torque Direct-Driven Permanent Magnet Synchronous Machines (PMSM) with Fractional-Slot Concentrated Winding Used in Coal Mine Belt Conveyor System. In Proceedings of the 2017 20th International Conference on Electrical Machines and Systems (ICEMS), Sydney, NSW, Australia, 11–14 August 2017; pp. 1–5.
11. Xu, X.H.; Zhou, G.H.; Rao, J.; Gao, Y. Study and Design of Low-Speed Direct-Driven Permanent Magnet Synchronous Machines (PMSM) for Fan Used on Power Air Cooling Island. In Proceedings of the 2017 20th International Conference on Electrical Machines and Systems (ICEMS), Sydney, NSW, Australia, 11–14 August 2017; pp. 1–5.
12. Feng, Y.J.; Li, F.; Huang, S.D.; Yang, N. Variable-Flux Outer-Rotor Permanent Magnet Synchronous Motor for in-Wheel Direct-Drive Applications. *Chin. J. Electr. Eng.* **2018**, *4*, 28–35.
13. Reichert, T.; Kolar, J.W.; Nussbaumer, T. Stator Tooth Design Study for Bearingless Exterior Rotor PMSM. *IEEE Trans. Ind. Appl.* **2013**, *49*, 1515–1522. [CrossRef]
14. Artetxe, G.; Paredes, J.; Prieto, B.; Martinez-Iturralde, M.; Elosegui, I. Optimal Pole Number and Winding Designs for Low Speed–High Torque Synchronous Reluctance Machines. *Energies* **2018**, *11*, 128. [CrossRef]
15. Soyaslan, M.; Avsar, Y.; Fenercioglu, A.; Eldogan, O. Cogging Torque Reduction in External Rotor PM Synchronous Motors by Optimum Pole Embrace. In Proceedings of the 2019 3rd International Symposium on Multidisciplinary Studies and Innovative Technologies (ISMSIT), Ankara, Turkey, 11–13 October 2019; pp. 1–4.
16. Minami, S.; Sanada, M.; Morimoto, S.; Inoue, Y. Influence of Ratio of External Diameter to Stack Length on Torque and Efficiency in Outer Rotor SPMSMs. In Proceedings of the 2015 IEEE Energy Conversion Congress and Exposition (ECCE), Montreal, QC, Canada, 20–24 September 2015; pp. 1834–1839.
17. Cui, J.G.; Xiao, W.S.; Wang, L.H.; Feng, H.; Zhao, J.B.; Wang, H.Y. Optimization Design of Low-Speed Surface-Mounted PMSM for Pumping Unit. *Int. J. Appl. Electromagn. Mech.* **2014**, *46*, 217–228. [CrossRef]
18. Fang, H.Y.; Qu, R.H.; Li, J.; Bao, S. Rotor Eddy-Current Loss Minimization in High-Speed PMSMs. In Proceedings of the 2016 IEEE Energy Conversion Congress and Exposition (ECCE), Milwakuee, WI, USA, 18–22 September 2016; pp. 1–8.
19. Ionel, D.M.; Popescu, M.; Dellinger, S.J.; Miller, T.J.E.; Heideman, R.J.; McGilp, M.I. On the Variation with Flux and Frequency of the Core Loss Coefficients in Electrical Machines. *IEEE Trans. Ind. Appl.* **2006**, *42*, 658–667. [CrossRef]
20. Pei, R.L.; Zhang, X.J.; Zeng, B.B.; Li, S.H. Studies of High-Frequency Iron Core Loss for Synchronous Electric Machines Used in Electric Vehicles. In Proceedings of the 2017 20th International Conference on Electrical Machines and Systems (ICEMS), Sydney, NSW, Australia, 11–14 August 2017; pp. 1–4.
21. Hao, J.; Suo, S.; Yang, Y.; Wang, Y.; Wang, W. Power Density Analysis and Optimization of SMPMSM Based on FEM, DE Algorithm and Response Surface Methodology. *Energies* **2019**, *12*, 3639. [CrossRef]
22. Song, T.F.; Zhang, Z.; Liu, H.; Hu, W. Multi-objective optimization design and performance comparison of permanent magnet synchronous motor for EVs based on FEA. *IET Electr. Power Appl.* **2019**, *13*, 1157–1166. [CrossRef]
23. Anders, G.; Prakashraj, K.T. Force Density Limits in Low-Speed PM Machines Due to Temperature and Reactance. *IEEE Trans. Energy Convers.* **2004**, *19*, 518–525.
24. Rafiee, V.; Faiz, J. Robust Design of an Outer Rotor Permanent Magnet Motor Through Six-Sigma Methodology Using Response Surface Surrogate Model. *IEEE Trans. Magn.* **2019**, *55*, 8107110. [CrossRef]